Electronic Supplementary Information
Increasing Hybridization Rate and Sensitivity of DNA Microarrays Using Isotachophoresis

Crystal M. Han,[1] Evaldas Katilius,[2] and Juan G. Santiago[1]
[1] Department of Mechanical Engineering, Stanford University, CA 94305, USA.
[2]SomaLogic Inc.,CO 80301, USA.

Contents
S1. Materials and reagents
S2. Geometry of microarray and microchannel device
S3. Visualization of ITP zones
S4. Effect of electric field on the sensitivity of ITP hybridization assay
S5. Experimental measurements of ITP parameters
S6. Additional data from titration experiments
S7. Limit of detection and repeatability

Table S1. Probe and target oligonucleotide sequences
Table S2. Coefficient of variation (CV) for the titration data in Figure 3

Figure S1. Microarray and microchannel geometry
Figure S2. Images of ITP zone at three sections of the channel
Figure S3. Effect of electric field and off-rate constant on ITP hybridization sensitivity
Figure S4. Experimental estimation of preconcentration and residence time
Figure S5. Additional titration data

S1. Materials and reagents

Sequences of all of the target and capture probe DNA oligonucleotides we used are listed in Table S1. Capture probes were synthesized with amino modifier with C6 and hexa-ethylene glycol linker (HEG) on 5' end. The amino modifier forms irreversible covalent bond with the epoxy group on the glass substrate, and HEG creates space between the oligonucleotide and the glass surface. Targets were modified with fluorescent dye Cy3 at the 5' terminus. Each probe-target pair had the same length and perfectly complementary sequence.

Table S1. Probe and target oligonucleotide sequences

Name	Probe sequence (5'→3')	Target Sequence (5'→3')	Length (mer)
1	GGGTCCCATATCCGAAACCCAGCTCA	TGAGCTGGGTTTCGGATATGGGACCC	26
2	TGTTCCTTTTCGTCCATTTAGTCAACC	GGTTGACTAAATGGACGAAAAGGAACA	27
3	GCCAAGTTGGCCAAGCAGCG	GCCAAGTTGGCCAAGCAGCG	20
4	TGTTCCCTCACGTCGCTCACAAACC	GGTTTGTGAGCGACGTGAGGGAACA	25
5	CTGGCTTAAATGGATTCGTCGGTGC	GCACCGACGAATCCATTTAAGCCAG	25
6	CTGGCCGTTGTCAGCGTGAAACATT	AATGTTTCACGCTGACAACGGCCAG	25
7	CTGTGAAAACACCGAGAAGCAGCCA	TGGCTGCTTCTCGGTGTTTTCACAG	25
8	CTGGCTAGATATAAACGCAAATTGC	GCAATTTGCGTTTATATCTAGCCAG	25
9	GTGTCTAATACTCAATCCAAGGGGC	GCCCCTTGGATTGAGTATTAGACAC	25
10	TCCTCTGTCCATAACCAGGATCAAA	TTTGATCCTGGTTATGGACAGAGGA	25
11	TGTTCCACACTCGTCAGGCGTGGAC	GTCCACGCCTGACGAGTGTGGAACA	25
12	TGTTCAGTGCCAGCTTAGAGCCAGG	CCTGGCTCTAAGCTGGCACTGAACA	25
13	CGGTGAACACTATTTCTAACTCTCA	TGAGAGTTAGAAATAGTGTTCACCG	25
14	TTGTGGTGTCTACGACTACTGAAAGC	GCTTTCAGTAGTCGTAGACACCACAA	26
15	AACCACGTGGCAATTAAAGAGAGCT	AGCTCTCTTTAATTGCCACGTGGTT	25
16	TGGTCAACACATAAGGACGTAGCCC	GGGCTACGTCCTTATGTGTTGACCA	25
17	GTGTCTCGACAATGTGCCAAAAGC	GCTTTTGGCACATTGTCGAGACAC	24
18	CTGTGTAGACATCGGATACGACCGC	GCGGTCGTATCCGATGTCTACACAG	25
19	TGTTCCATTTGGCTCACAACATGAA	TTCATGTTGTGAGCCAAATGGAACA	25
20	CGGTCTTCCTGCCACACCAACCCTC	GAGGGTTGGTGTGGCAGGAAGACCG	25

S2. Geometry of microarray and microchannel device

Our system consisted of custom-printed microarrays on glass slides. As mentioned in the main text, the microarrays were printed by Applied Microarrays, Inc. (AMI, Tempe, AZ). We fabricated small PDMS microchannel superstructures which we then bonded to these arrays. Figure S1 shows details of microarray and microchannel geometry. Shown is a drawing of the channels of the PDSM superstructure and a superposed image of the microarray (shown as a gray rectangle). On a standard size (25 mm by 75 mm) glass slide, we had printed six blocks of identical microarrays. Each block consisted of a total 160 spots of 20 sequences (with 8 replicates). Our microchannel was nominally 500 μm wide, 80 mm long and 40 μm deep, except for a middle portion, which had a smooth transition to and from a 200 μm wide (at the throat) constriction immediately upstream of the microarray sites. 90 degree low-dispersion turns were used on the corners.[1]
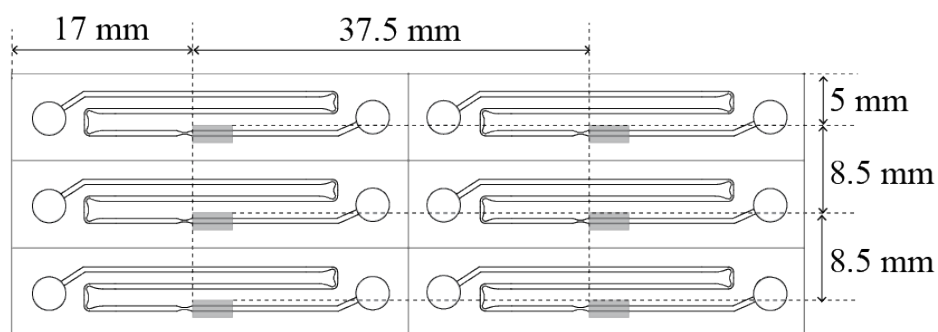
Figure S1. Drawing of glass microarray and PDMS microchannel superstructure. On each slide, the glass substrate contained 6 identical printed microarrays. To each array, we bonded a PDMS superstructure which formed a microchannel leading to and from of the array. Gray rectangles indicate the location of microarray blocks. Each DNA array had horizontal and vertical dimensions of approximately 4 and 1.5 mm. Left and right circles respectively indicate TE (input) and LE (output) reservoirs, where aqueous TE containing targets and gel-phase LE (LE2) were loaded and electrodes were placed. The width of microchannel is nominally 500 μm, except at a 500 μm long constriction region where the channel tapered down to a smooth 200 μm wide "throat" constriction with fore aft symmetry.

S3. Visualization of ITP zones

We here present images of ITP zones at three sections of the channel: before the constriction, at the constriction, and after the constriction. These images serve as the experimental visualization of the steps described in the schematic in the Figure 1a. These images are taken from an independent, preliminary ITP experiment with a mixture of targets but no microarray. At the focusing step, we applied high electric field (1100 V along the channel) to obtain fast accumulation of targets at the ITP zone. As shown in Figure S2, we observed the characteristics of electrokinetic instabilities such as asymmetric distribution of focused analytes and temporal fluctuations.[2] Once the ITP zone entered the tapered zone, we deactivated the electric field, and waited for 2 min to allow molecular diffusion to homogenize the target concentration within the narrow constriction. Assuming a diffusion coefficient of 9.2×10^{-10} m^2/s,[3,4] the characteristic diffusion time for 200 μm wide constriction is estimated as 40 s. As expected we observed negligible non-uniformity of concentration after 2 min of diffusion. We then re-activated electric field at a lower magnitude. At the lower current, we believe that we do not exceed the threshold for the onset of electrokinetic instability.[2] Thus we observed the ITP zone slowly migrated downstream (where immobilized probes are supposed to be located) maintaining the uniform distribution in the span-wise direction of the channel.
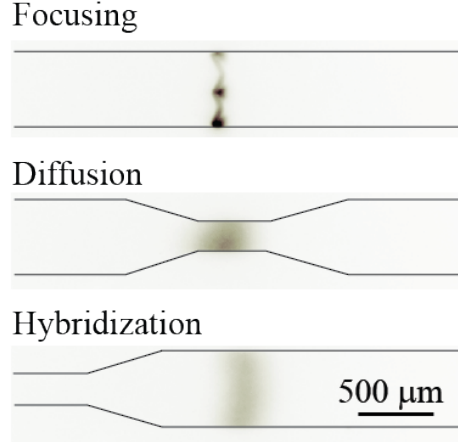
Focusing

Diffusion

Hybridization

500 μm

Figure S2. Images of ITP zones at three sections of our channel. We used TE including mixture of 1 nM targets and PDMS channel with no immobilized probes for this independent ITP experiment. The images were taken from a single ITP experiment. During the initial focusing, rapid-accumulation step, we observed non-uniform distribution of targets migrating at a high velocity. After the zone arrived the constriction, we deactivated the electric field to allow diffusion to homogenize the target concentration. The middle "Diffusion" image was taken approximately 20 s after the field is deactivated. After 2 min, we re-applied the electric field at a lower current, and observed the slow migration of ITP zone with uniform span-wise concentration profile.

S4. Effect of electric field on the sensitivity of ITP hybridization assay

As discussed in the main paper, the absolute calibration between the fraction of hybridized probes and the initial target concentration is a function of parameters describing the degree of ITP focusing and ITP zone velocity. Specifically, the binding reaction is a function of the preconcentration factor p, the ITP zone width δ_{ITP}, and the ITP zone velocity V_{ITP}. Each of these parameters is a function of the applied electric field. We here present an approximate analysis of the hybridization reaction dynamics as a function of the electric field (an independent parameter in this problem). Electric field is an important experimental parameter as it is perhaps the easiest to vary. Here we use our buffer composition (see Materials and Methods section of main paper) as an example condition to explore the effect of the electric field. In the main paper, we derived an ITP hybridization model as a function of ITP parameters which are experimentally measurable. This model can be summarized as follows:

$$h_{ITP} = \frac{pC_0^*}{pC_0^* + 1}(1 - \exp(-(pC_0^* + 1)\frac{\delta_{ITP}}{V_{ITP}}k_{off})). \tag{1}$$

We can express the key variables V_{ITP}, δ_{ITP}, and p each in terms of applied electric field according to classical analytical ITP theory. Assuming strong suppression of bulk flow, the ITP zone velocity is given as

$$V_{ITP} = \mu_{LE}E. \tag{2}$$

where E is electric field in the portion channel filled with the LE buffer, and μ_{LE} denotes effective mobility of the LE ion. Under constant current conditions, the value of E does not change as the ITP zone migrates, resulting in a constant ITP velocity during the

assay. This is important for ITP hybridization of microarray to ensure similar hybridization dynamics for all spots. Following MacInnes and Longsworth's,[5] we can estimate the ITP zone width (for molecular diffusion-limited ITP zone widths) using the following analytical expression:

$$\delta_{ITP} = \frac{RT}{FV_{ITP}}\left(\frac{\mu_{LE}\mu_{TE}}{\mu_{LE} - \mu_{TE}}\right),$$ (3)

where R is the universal gas constant, T is the absolute temperature, and F is Faraday's constant. This relation assumes the focused target molecules are in peak mode with a mobility sufficiently greater than that of the TE co-ion and sufficiently lower than the LE co-ion.[6,7] We can express the accumulate rate of target species in peak mode ITP using the model of Khurana et al.,[8] Based on Khurana's analysis, we estimate the preconcentration level of the analyte as

$$p = \left(\frac{\mu_A}{\mu_{TE}} - 1\right)\frac{\mu_{TE}}{\mu_{LE}}\frac{\mu_{CI} - \mu_{LE}}{\mu_{CI} - \mu_{TE}}\frac{c_{LE}}{c_{TE}}\frac{L}{\delta_{ITP}}$$ (4)

where L is migration length, and δ is ITP width we define in the equation (3). Here, subscripts 'TE', 'LE', and 'CI' denote respectively the properties related to the trailing, leading ions, and the counter ion. c_{LE} and c_{TE} respectively denote concentrations of LE and TE buffers in the reservoirs. Finally, we substitute the expressions from Equation (2-4) for V_{ITP}, δ_{ITP}, and p in our ITP hybridization model. We summarize the model parameters here for convenience: $\mu_{TE} = 21 \times 10^{-9}$ m^{2}V^{-1}s^{-1}, $\mu_A = 35 \times 10^{-9}$ m^{2}V^{-1}s^{-1}, $\mu_{CI} = 9 \times 10^{-9}$ m^{2}V^{-1}s^{-1}, $C_0^* = 10^{-4}$, $L = 0.06$ m.

In Figure S3, we present contours of the ratio of fraction of hybridized probes of ITP (h_{ITP}) to the fraction of hybridized of conventional hybridization at equilibrium (h_{eq}) as a function of applied electric field (abscissa) and kinetic off-rate constant (ordinate) values. The gray area in the plot represents the parameter values for which ITP yields higher sensitivity than conventional method. For a given k_{off}, we see that lower electric field results in more sensitivity improvement. Note that preconcentration is a linear function of E, while the ITP reaction time scales as $1/E^2$. As a consequence, lower electric field results in lower preconcentration but the stronger dependence of reaction time on electric field results in a higher fraction hybridized. In contrast to the case of sensitivity, ITP total assay time is inversely proportional to square of electric field. This indicates a strong trade-off between sensitivity and reaction time where the slight increases in sensitivity are offset by more increase in assay time.
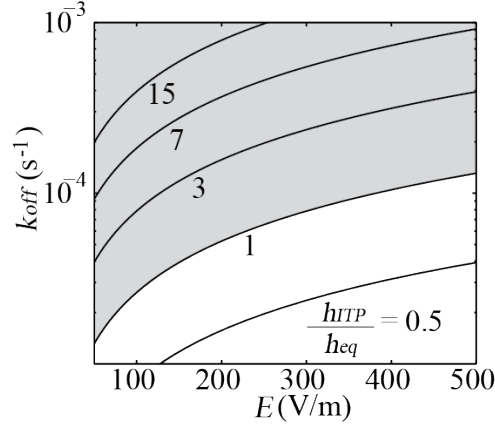
10^{-3}

15

7

10^{-4}

3

1

k_{off} (s^{-1})

$\dfrac{h_{ITP}}{h_{eq}} = 0.5$

100   200   300   400   500

E (V/m)

Figure S3. Contours representing the ratio of fraction of hybridized probes of ITP hybridization to that of conventional hybridization at equilibrium, h_{ITP} / h_{eq}, as a function of electric field E (abscissa) and dimensional kinetic off rate constant, k_{off}. For a typical range of electric field for ITP used here, we see sensitivity increases as electric field decreases. The parameter combination resulting in the ratio greater than 1 is indicated with gray color, implying that signal from ITP hybridization is higher than equilibrium signal of conventional experiments. We used estimates for ITP zone width and accumulation rates based on analytical models of ITP dynamics.

S5. Experimental measurements of ITP parameters

We here present a calibration curve and graphical representation of top-hat approximation of ITP zone in Figure S4. For these data, we used the same 1 s exposure time and an ICCD camera gain of 40. We recorded images of our microfluidic channel filled with twenty targets at concentration of 25, 50, and 100 nM mixed in LE1. We obtained a corrected image I_{corr} using the raw fluorescence image, buffer-only background image, and flat field image according to Equation (5) provided in the main manuscript. We then fit the experimental data with the linear polynomial to derive the relation $I_{corr} = 1.02 \times 10^{10} C_{T0} + 41$ where C_{T0} is the concentration of target (Figure S4a).

For measurements of ITP parameters, we conducted independent ITP experimnets with 2 μA constant current using 250 pM reservoir concentration. We applied the same image correction analysis to the ITP data. Then, the corrected intensity was averaged in the span-wise direction of the channel, and converted into concentration value using the calibration curve shown in Figure S4a. We fit our experimental data with the Gaussian distribution of the form $C = Ae^{(x-\mu)^2/2\sigma^2}$ where C is the concentration in the ITP zone, A is the amplitude, μ is the mean, and σ is the standard deviation. We defined the top-hat approximation with a characteristic ITP interface width, δ_{ITP}, and p-fold increased reservoir concentration, pC_{T0}. To this end, we set δ_{ITP} to be the $\pm 2\sigma$ width of the Gaussian peak. We determined the magnitude of the top-hat pulse, pC_{T0}, such that the area under the pulse, $4\sigma pC_{T0}$, equals to the area of the Gaussian peak, $\sqrt{2\pi}A\sigma$. We present the graphical representation of this in Figure S4b.
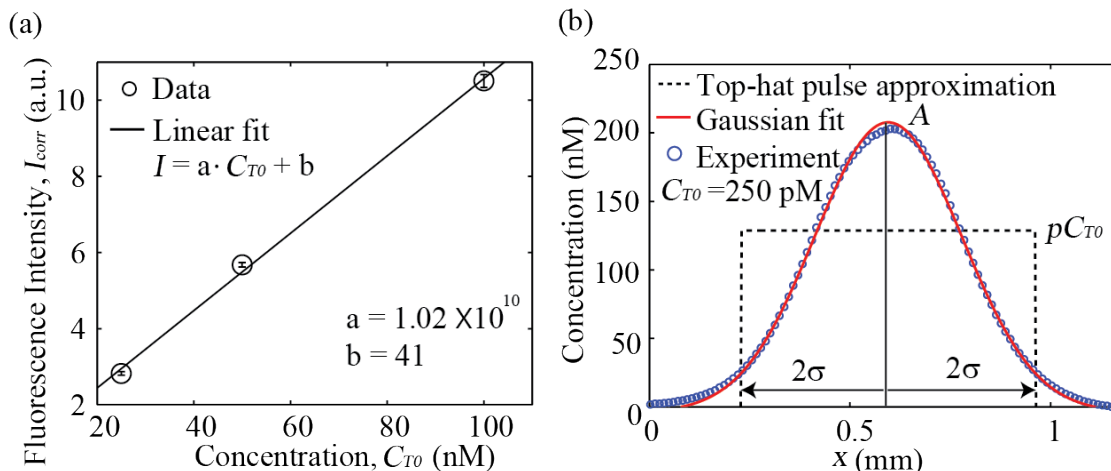
(a) (b)

Figure S4. (a) Calibration curve for the relation between fluorescence intensity and target concentration. All data was taken under the same imaging condition of 1 s exposure time and ICCD camera gain of 40. These uncertainty bars represent a standard deviation from 30 measurements. Least square fit was used to extract the linear relation found as $I_{corr} = 1.02 \times 10^{10} C_{T0} + 41$. (b) Top-hat pulse approximation of Gaussian-like ITP zone. Experiment was conducted using a 250 pM reservoir concentration, C_{T0}. The corrected intensity was averaged in the span-wide direction of microchannel, and converted to concentration value. The width and height of the pulse was defined as 4σ and $\sqrt{2\pi}A/4$ where A and σ respectively denote the magnitude and standard deviation of the Gaussian fit. Like this, ITP preconcentration and zone width were measured and averaged from five repetitions of ITP experiment.

S6. Additional data from titration experiments

We here include and discuss additional analyses of the experiments show in Figure 3 of the main paper. For these experiments, we used a mixture of twenty targets at concentrations ranging from 100 fM to 10 nM. In Figure S5, we present experimental data of fraction of hybridized probes for ITP (triangle) and conventional hybridization (circle) for targets 7, 12, 18, and 20 as comparisons to the case of target 1 shown in Figure 3. Shown with the experimental data are the theoretical models for ITP (solid lines) and conventional (dashed lines) hybridization. Similar to target 1, we observe good qualitative agreement of predicted trends and our experimental data. For each target, we used the same method to find fitting parameters K and k_{on}, and these species-specific values are shown in the figure legend. As expected from their similar lengths, the estimated kinetic parameters for these targets are on the same order as those for target 1. Note that these reaction parameters are also in the range of typical values reported for heterogeneous hybridization.[9–11]

The additional titration data in Figure S5 confirm a 4 orders of magnitude dynamic range of quantitative detection for the various sequences. Also the experimental data and theoretical model predictions in all cases demonstrate higher sensitivity for the 30 min ITP hybridization over 15 h conventional hybridization. We see that the level of sensitivity increase depends on the kinetic off-rate constant as expected from the analytical model (see Figure 2 in the paper). For example, the predicted sensitivity

increase for target 18 with smaller k_{off} value of 1.6×10^{-5} s^{-1} is 2-fold whereas target 20 with k_{off} value of 4.0×10^{-5} s^{-1} has the calculated sensitivity increase of about 5-fold. This difference in sensitivity increase is clearly reflected in the experimental hybridization data.
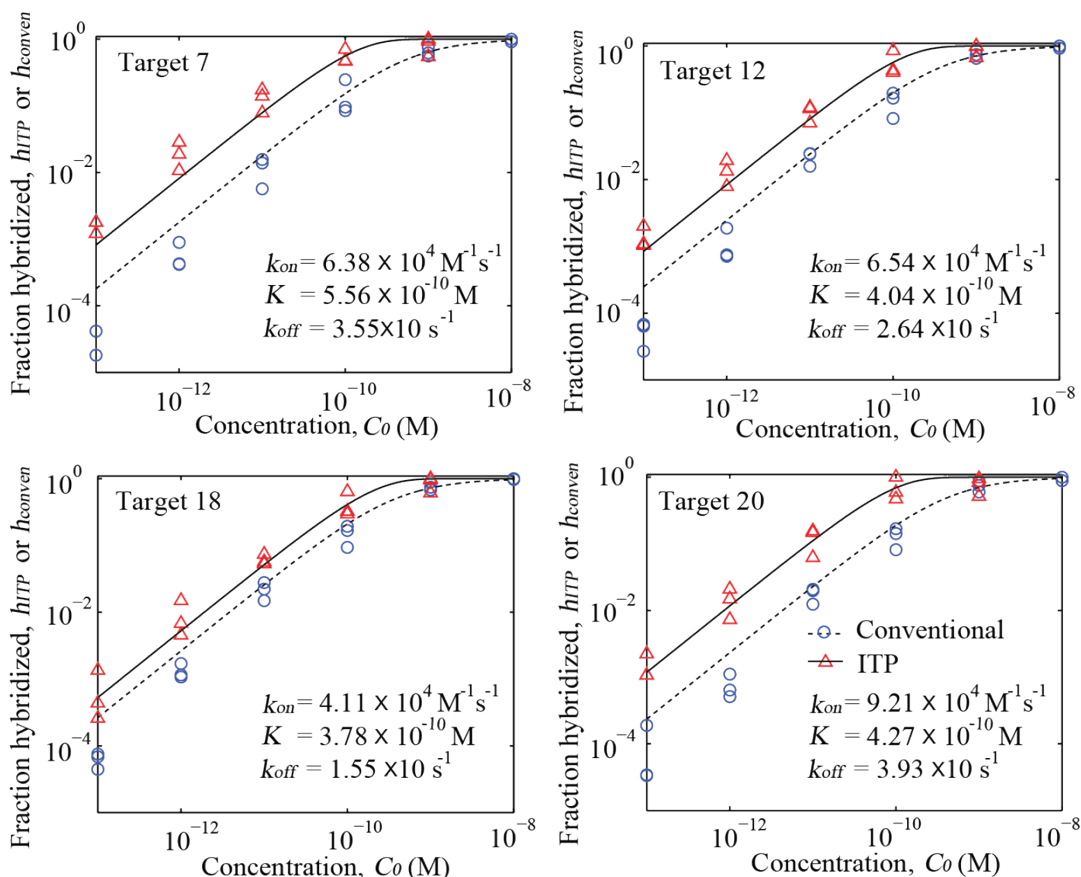

Figure S5. Titration curves of targets 7, 12, 18, and 20 for concentrations ranging from 100 fM to 10 nM. Experimental data for ITP hybridization is represented with triangles, and that for conventional hybridization is shown with circles. We used a single fitting parameter K for the conventional hybridization model (dashed line), and an additional parameter, k_{on}, for ITP hybridization model (sold line). In all cases, ITP shows enhanced sensitivity over the conventional hybridization, and the degree of enhancement is a function of k_{off} as expected.

S7. Limit of detection and repeatability

We determined the limit of detection (LOD) of for both conventional hybridization and ITP-aided hybridization based on the titration data presented in Figure 3 of the main paper. The spot fluorescence signal intensity and the local background intensity around the spot were extracted from GenePix Pro 6.0 software. We evaluated the LOD as the minimum target concentration which provided a signal-to-noise ratio (SNR) of 3. Here, we defined the 'signal' as the background subtracted intensity from each spot, and 'noise' as the standard deviation of the background signals from three repeats at each concentration. For conventional ITP, we calculated SNR values of

2.2 and 46.7 for target concentrations of 100 fM and 1 pM, respectively. Linear interpolation determined the LOD of the conventional hybridization to be approximately 120 fM. For ITP, the SNR at the lowest concentration we explored, 100 fM, was 40.7. Therefore, the LOD of ITP is approximately 10-fold lower than the conventional hybridization.

In Table S2, we present the coefficient of variation (CV) calculated as the standard deviation divided by the mean value of the three repetitions shown in Figure 3 per each concentration. The CV for conventional hybridization ranged from 0.16 to 0.59, and CV for ITP hybridization ranged from 0.14 to 0.37. These results suggest that ITP hybridization is similar to conventional hybridization in terms of reproducibility.

Table S2. Coefficient of variation (CV) for the titration data in Figure 3 (N = 3)

	100 fM	1 pM	10 pM	100 pM	1 nM
Conventional	0.26	0.56	0.41	0.59	0.16
ITP	0.14	0.37	0.25	0.23	0.26

References
1.   J. I. Molho, A. E. Herr, B. P. Mosier, J. G. Santiago, T. W. Kenny, R. a. Brennen, G. B. Gordon, and B. Mohammadi, *Anal. Chem.*, 2001, **73**, 1350–1360.
2.   A. Persat and J. G Santiago, *New J. Phys.*, 2009, **11**, 075026.
3.   A. E. Nkodo, J. M. Garnier, B. Tinland, H. Ren, C. Desruisseaux, L. C. McCormick, G. Drouin, and G. W. Slater, *Electrophoresis*, 2001, **22**, 2424–2432.
4.   V. Chan, D. J. Graves, and S. E. McKenzie, *Biophys. J.*, 1995, **69**, 2243–2255.
5.   D. A. MacInnes and L. G. Longsworth, *Chem. Rev.*, 1932, **11**, 171–230.
6.   G. Garcia-Schwarz, M. Bercovici, L. a. Marshall, and J. G. Santiago, *J. Fluid Mech.*, 2011, **679**, 455–475.
7.   S. Rubin, O. Schwartz, and M. Bercovici, *Phys. Fluids*, 2014, **26**, 012001.
8.   T. K. Khurana and J. G. Santiago, *Anal. Chem.*, 2008, **80**, 6300–6307.
9.   K. Tawa and W. Knoll, *Nucleic Acids Res.*, 2004, **32**, 2372–2377.
10. M. R. Henry, P. Wilkins Stevens, J. Sun, and D. M. Kelso, *Anal. Biochem.*, 1999, **276**, 204–214.
11. Y. Okahata, M. Kawase, K. Niikura, F. Ohtake, H. Furusawa, and Y. Ebara, *Anal. Chem.*, 1998, **70**, 1288–1296.